THE ASTROPHYSICAL JOURNAL, 461:115–126, 1996 April 10

RADIO JETS AND THE FORMATION OF ACTIVE GALAXIES: ACCRETION AVALANCHES ON THE TORUS BY THE EFFECT OF A LARGE-SCALE MAGNETIC FIELD

R. MATSUMOTO,[1,2] Y. UCHIDA,[3,4] S. HIROSE,[3] K. SHIBATA,[5] M. R. HAYASHI,[6] A. FERRARI,[7,8] G. BODO,[8] AND C. NORMAN[9]

Received 1994 November 21; accepted 1995 October 26

ABSTRACT

We present the results of 2.5-dimensional MHD simulations for a magnetohydrodynamic model of jet formation associated with the formation of active galaxies. We also study the enhanced accretion near the central object of active galactic nuclei. A new factor introduced in our model is the presence of a large-scale poloidal magnetic field that may correspond to either the primordial magnetic field swept into the central region during the galaxy formation process or the central part of a dynamo-generated magnetic field. The differentially rotating disk produced around a central massive object such as a black hole interacts with the large-scale magnetic field, and produces spinning bipolar jets through the production and escape of the magnetic twists propagating into bipolar directions (a form of large-amplitude torsional Alfvén waves). The production and escape of these removes angular momentum from the disk material and allows an enhanced accretion rate in the disk. The surface layers of disks accrete faster than the equatorial part because the magnetic braking most effectively affects that layer. The infalling gas spins up, and jet formation strengthens until magnetic reconnection occurring at the inner edge of the disk saturates the process.

Subject headings: accretion, accretion disks — galaxies: active — galaxies: jets — MHD

1. INTRODUCTION

Well-collimated energetic jets from active galactic nuclei (AGNs) and quasars have been attributed in many models to powerful winds thought to be collimated and accelerated when passing through the funnel of an accretion disk surrounding a central massive black hole (see, e.g., Lynden-Bell 1978; Fukue 1982; Begelman, Blandford, & Rees 1984). Some other models claim that jets are created essentially by magnetic mechanisms: they are created from the rotating disk surrounding a black hole by the action of a large-scale magnetic field (see, e.g., Blandford & Payne 1982; Uchida & Shibata 1985; Shibata & Uchida 1986; Sakurai 1987; Lovelace, Wang, & Sulkanen 1987).

Blandford & Payne (1982) discussed the centrifugal acceleration of gas in a rigid magnetic flux tube fanning out from the disk and bending toward the polar directions. The magnetic field is rotated with its shape fixed relative to the rotating disk up to the Alfvén point. Gas entrained into the flux tube is accelerated by the centrifugal effect. Pudritz & Norman (1983) applied it to the star formation case. Further detailed work has been done on the asymptotics by Heyvaerts & Norman (1989). The mass flux of the steady magnetically driven jets can be determined by requiring the solution to pass through the slow magnetosonic point smoothly (see, e.g., Cao & Spruit 1994; Li 1995). By assuming the shape of poloidal magnetic field lines, Kudoh & Shibata (1995) showed that for a wide range of parameters the terminal velocity of such steady solutions is an order of Keplerian velocity at the footpoint of the jets.

The shape of the magnetic field lines for the axisymmetric steady ideal MHD flow should be determined in such a way that the force balance across the field is satisfied. Such self-consistent solutions have been obtained numerically by Sakurai (1987) for nonrelativistic jets (see Camenzind 1987 for the relativistic case). Semianalytic self-similar solutions have been given by Contopoulos & Lovelace (1994) for the generalized Grad-Shafranov equation (Lovelace et al. 1986) for axisymmetric ideal MHD flow. More recently, Li (1995) obtained self-similar steady axisymmetric solutions including both the wind and the disk by assuming turbulent magnetic diffusivity inside the disk (see also Lubow, Papaloizou, & Pringle 1994a, b and Lovelace, Romanova, & Newman 1994).

Uchida & Shibata (1985) showed that another type of magnetic mechanism works (they called this process a "sweeping magnetic twist mechanism") for the acceleration of jets. They first studied the star formation case and later extended their mechanism to the case of AGN jets (Uchida & Shibata 1986; Uchida et al. 1991). Their treatment was based on 2.5-dimensional (axisymmetric, but allowing the φ components of vector quantities) numerical simulations solving a full set of MHD equations, containing all possible actions of magnetic fields.

The characteristic features of the jets predicted in their mechanism—(1) a hollow cylindrical structure, (2) a long-ranged acceleration, and (3) a helical velocity field in the jet (or bipolar flow lobes in the case of the star formation bipolar flows)—were actually found in the observations in the ^{12}CO $J = 1$–0 line of the bipolar flow lobes in L1551 (Uchida et al. 1987), favoring their magnetic model, rather than the previously believed funnel collimation pictures.

[1] Department of Physics, Faculty of Science, Chiba University, Inage-ku, Chiba 263, Japan; matumoto@c.chiba-u.ac.jp.
[2] Advanced Science Research Center, JAERI, Naka, Japan.
[3] Department of Physics, Science University of Tokyo, Shinjuku-ku, Tokyo 162, Japan.
[4] Department of Astronomy, University of Tokyo, Bunkyo-ku, Tokyo 113, Japan.
[5] National Astronomical Observatory, Mitaka, Tokyo 181, Japan.
[6] Department of Physics, Graduate School of Science and Technology, Chiba University, Inage-ku, Chiba 263, Japan.
[7] Institute of General Physics, University of Torino, Torino, Italy.
[8] Osservatorio Astronomico di Torino, I-10025 Pino Torinese, Italy.
[9] Department of Physics and Astronomy, Johns Hopkins University and Space Telescope Science Institute, Baltimore, MD 21218.

The spinning of the lobes is especially difficult to explain in terms of previous nonmagnetic models, which assumed that the wind from the central object was collimated by the funnels that opened up along the rotation axis of the accretion disk. This is because the pointlike central source of the wind does not have an appreciable amount of angular momentum, and even if it had, no appreciable angular momentum is transported if there is no mechanism like the magnetic tension.

The Uchida-Shibata model deals with the disk in a fully dynamical way, allowing a realistic response of the disk to the formation of jets. Their model explains the enhancement of accretion of the disk material to the central body by the magnetic braking due to the loss of angular momentum in the production of magnetically accelerated spinning jets. The enhanced angular momentum transfer increases the accretion rate and correspondingly enhances the energy generation.

The amplification of the toroidal magnetic field by differential rotation and the enhanced accretion by magnetic braking can be considered a dynamical dynamo process (Uchida et al. 1996). Here we note that the dynamical dynamo process involved in the Uchida-Shibata model is closely related to the Balbus & Hawley (or Velikhov & Chandrasekhar) instability (Velikhov 1959; Chandrasekhar 1961; Balbus & Hawley 1991), which has been studied extensively (see, e.g., Balbus & Hawley 1991, 1992; Hawley & Balbus 1991, 1992; Tagger, Pellat, & Coroniti 1992; Vishniac & Diamond 1992; Tout & Pringle 1992) since Balbus & Hawley (1991) pointed out its importance in magnetized accretion disks. When the effect of gravitational stratification of the disk is included for disks threaded by large-scale poloidal magnetic fields, as in the Uchida-Shibata model, the torsional Alfvén waves that cause the Balbus & Hawley instability propagate through the low-density part of the disk in bipolar directions outside the disk along the poloidal magnetic field, swirling up the matter from the disk into helical jets as well as extracting the angular momentum of the disk. Stone & Norman (1994) confirmed the numerical results of Uchida & Shibata (1985) and Shibata & Uchida (1986) by using the ZEUS-2D code (Stone & Norman 1992a, b).

Several authors have attempted to get a quasi-steady state solution of magnetically driven jets by dynamically evolving the disk-wind system for more than 20 rotations with a boundary condition that magnetic fields are anchored on the equatorial disk, which rotates with a fixed Keplerian speed (Ustyugova et al. 1995; Kudoh & Shibata 1996). The effects of magnetic braking have not been fully taken into account in these models.

In the present paper, we examine the back-reaction of magnetic jet production in more detail by using the geometrically thick accretion disk model (see, e.g., Abramowicz, Jaroszynski, & Sikora 1978). Although thick accretion disks have been found to be unstable against the non-axisymmetric perturbations (Papaloizou & Pringle 1984), realistic inflowing inner boundary conditions can cut off the amplification of the instability due to waves not being reflected from the inner boundary (Blaes 1987).

In § 2 we describe briefly the astrophysical situation we deal with. In § 3 the basic equations, the numerical method, and the boundary conditions are given. The results of simulations by our 2.5-dimensional MHD code are presented in § 4. Relations between the enhanced rate of accretion and the rate of angular momentum loss due to the jet formation (emission of large-amplitude torsional Alfvén waves causing a helical jet) are discussed together with their astrophysical significance. Last, overall discussions are given in § 5.

2. THE ESSENTIAL COMPONENT OF THE MODEL

In the following, we assume that a massive black hole with, say, $M \sim 10^9\, M_\odot$ is located at the center of a protogalaxy. A gas disk and outer torus is assumed to encircle the massive central object. The system of central massive object, disk, and torus is assumed to sweep up a part of the large-scale poloidal magnetic flux in the process of formation. The large-scale poloidal magnetic field assumed here may either be a part of the primordial magnetic field (Kulsrud & Andersen 1992) brought into the central part of the protogalaxy in the process of its formation or swept into the central regions of a merging galaxy system so often found to be associated with active galaxies and starbursts, or it may be the central part of the dynamo-generated global magnetic field system, which can be regarded as a large-scale poloidal magnetic field with respect to our very small system of central massive object, accretion disk, and torus at the center. In both possibilities the central part of the large-scale poloidal field will be bunched further in the process of accretion of mass into the black hole plus disk system and acquire an hourglass-shaped configuration (Uchida & Shibata 1985). The axis of rotation of the disk is likely to be parallel to the large-scale magnetic field because the angular momentum components perpendicular to the large-scale magnetic field are likely to be damped in the earlier phase of contraction (Mestel 1972).

Here let us compare the timescale of matter infall and the field rearrangements. When the infalling matter enters the radius of influence of the black hole $r_h \sim GM_h/\sigma^2$, where σ^2 is the depth of the potential well of the galaxy, the characteristic infall timescale is r/v_k, where r is the distance from the central black hole and v_k is the Keplerian velocity. If during the collapse (or sweeping due to merging) $B \propto n^\alpha$, where $\alpha = \frac{1}{2}$–$\frac{2}{3}$, then $v_A = v_{A0}(n^\alpha/n^{1/2}) = v_{A0}\, n^{\alpha'}$, where $\alpha' = 0$–$\frac{1}{6}$. The ratio of the timescale for infall $t_{\rm infall} \sim r/v_k$ and the timescale for the rearrangement of magnetic fields $t_B \sim r/v_A$ is $t_{\rm infall}/t_B = v_A/v_k \ll 1$.

The hourglass-shaped magnetic field will be twisted up by the differentially rotating disk located at its throat, since different parts of the curved magnetic field embedded in the disk are carried around the axis with different angular velocity and the azimuthal field component, B_φ, is produced continuously. As the twist is accumulated near the surface layer of accretion disks, it relaxes out along the poloidal field into the bipolar directions in the form of nonlinear torsional Alfvén waves. These relaxing magnetic twists entrain the low-density part of the disk material in the form of spinning jets toward the bipolar directions as they propagate through the disk atmosphere in the form of nonlinear torsional Alfvén waves (Uchida & Shibata 1985). This occurs outside the region where the Alfvén velocity, which increases as the height in the disk atmosphere increases, becomes comparable to the local free-fall velocity, and brings the plasma into a helical motion before it slides down along the field lines.

Applications of this mechanism to the problem of the radio jets and lobes from AGNs have been made by noting a similarity law (Uchida & Shibata 1986) of the magnetohydrodynamic equations for such systems: The non-

dimensionalized system of equations will have an exactly similar solution if the nondimensional coefficients appearing in the nondimensionalized equation system (three ratios of four nondimensionalized forces, pressure, magnetic, centrifugal, and gravity), as well as the initial situations in the scaled coordinate, are the same.

Of course, the correspondence of star formation and central massive object formation in the galactic center will not be exactly similar, but these two may be said to be conceptually similar, having the central gravitator and a disk surrounding it. The three ratios of nondimensional forces turn out to be in the similar range of values. The principal differences between the two calculations is that jets in AGNs are usually relativistic and in star formation cooling is dominant. It is remarked that the reaction of the production of the jets may exert magnetic braking to the disk, as in the case of the star formation jet, and may cause enhanced accretion of the disk material, and therefore may explain the enhancement of the liberation of the gravitational energy of the AGN itself.

3. BASIC EQUATIONS, NUMERICAL METHODS, AND INITIAL MODELS

3.1. *Basic Equations*

The equation system we use is that for ideal magnetohydrodynamics with an adiabatic energy equation for simplicity, in a cylindrical coordinate (r, φ, z):

$$\frac{\partial \rho}{\partial t} + \nabla(\rho \boldsymbol{v}) = 0 , \tag{1}$$

$$\frac{\partial}{\partial t}(\rho v_r) + \nabla(\rho v_r \boldsymbol{v}) - \frac{\rho v_\varphi^2}{r} + A_1 \frac{\partial p}{\partial r} - \frac{A_2}{4\pi}[(\nabla \times \boldsymbol{B}) \times \boldsymbol{B}]_r - A_3 \rho g_r = 0 , \tag{2}$$

$$\frac{\partial}{\partial t}(\rho v_z) + \nabla(\rho v_z \boldsymbol{v}) + A_1 \frac{\partial p}{\partial z} - \frac{A_2}{4\pi}[(\nabla \times \boldsymbol{B}) \times \boldsymbol{B}]_z - A_3 \rho g_z = 0 , \tag{3}$$

$$\frac{\partial}{\partial t}(r\rho v_\varphi) + \nabla(r\rho v_\varphi \boldsymbol{v}) - \frac{A_2}{4\pi}\nabla(rB_\varphi \boldsymbol{B}) = 0 , \tag{4}$$

$$\frac{\partial \boldsymbol{B}}{\partial t} - \nabla \times (\boldsymbol{v} \times \boldsymbol{B}) = 0 , \tag{5}$$

$$\left(\frac{\partial}{\partial t} + \boldsymbol{v} \cdot \nabla\right)(p\rho^{-\gamma}) = 0 , \tag{6}$$

where $\boldsymbol{g} = -\nabla\phi$, $\phi = -(r^2 + z^2)^{-1/2}$,

$$A_1 = v_{s0}^2/(\gamma v_{\varphi 0}^2) , \quad A_2 = v_{A0}^2/v_{\varphi 0}^2 , \quad A_3 = v_{K0}^2/v_{\varphi 0}^2 ,$$

$$v_{s0}^2 = \gamma R T_0 , \quad v_{A0}^2 = B_0^2/(4\pi\rho_0) , \quad \text{and} \quad v_{K0}^2 = GM/r_0 .$$

In these equations, ρ, p, and T are the density, pressure, and temperature, $\boldsymbol{v}$ is the velocity of the gas, $\boldsymbol{B}$ is the magnetic field, $\boldsymbol{g}$ and ϕ are gravitational force and potential, respectively, with G the gravitational constant, M the mass of the central object, R the gas constant, and γ the ratio of specific heats. The nondimensional coefficients A_i are as defined, with v_s, v_A, v_K, and v_φ the acoustic, Alfvén, Keplerian, and rotational velocities, respectively. The subscript 0 signifies the values at a given point $(r_0, 0, 0)$ in the disk. All the quantities are normalized by their values with subscript 0, as in $\rho' = \rho/\rho_0$, etc., and the primes are omitted altogether. The scaling of time is $r_0/v_{\varphi 0}$.

3.2. *Numerical Method and Boundary Conditions*

The numerical method we use is a modified Lax-Wendroff scheme with artificial viscosity for 2.5-dimensional MHD problems in cylindrical geometry, which was already used in the simulations in the context of star formation (Uchida & Shibata 1985; Shibata & Uchida 1986, 1990). Since axisymmetry is not a reasonable approximation when turbulent processes become important, the applicability of our 2.5-dimensional (axisymmetric) MHD simulation is limited when the disk becomes turbulent, owing to the growth of nonaxisymmetric instabilities. Three-dimensional global MHD simulations of magnetized accretion torus are now in progress to study the nonlinear growth of instabilities such as the nonaxisymmetric Balbus & Hawley instability (see Hawley, Gammie, & Balbus 1995, Matsumoto & Tajima 1995, and Brandenburg et al. 1995 for local three-dimensional MHD simulations). We confirmed that three-dimensional global MHD simulations with imposed nonaxisymmetric perturbations at $t = 0$ give essentially the same results as 2.5-dimensional simulations up to the stage we report in this paper (one rotation at $r = r_0$). This coincidence with axisymmetric simulations occurs because nonaxisymmetric instabilities need several rotation periods before their amplitudes grow large enough to modify the disk structure and the angular momentum distribution. Thus, in the following, we focus on the axisymmetric evolution of a magnetized torus. The results of longer timescale three-dimensional global simulations will be reported in subsequent papers (Matsumoto et al. 1996). Another limitation of the applicability of our numerical scheme appears when the magnetic field at the inner edge of the disk grows too strong and the Alfvén velocity becomes very large in this region since the Courant condition forces a very small time step.

Boundary conditions taken on the boundaries of our r-z plane are as follows: At the equatorial plane ($z = 0$), we assume a boundary condition that is symmetric for density, pressure, v_r, v_φ, and B_z but antisymmetric for v_z, B_r, and B_φ. On the axis ($r = 0$), density, pressure, v_z, and B_z are symmetric, while v_r, v_φ, B_r, and B_φ are antisymmetric. The side surface, $r = R_{max}$, and the top surface, $z = Z_{max}$, are free boundaries at which the mass as well as waves can go through freely, and we set $\partial \delta Q/\partial z = 0$ on $z = Z_{max}$ and $\partial \delta Q/\partial r = 0$ on $r = R_{max}$, where Q is one of the above variables, and $\delta Q \equiv Q(r, z, t + \delta t) - Q(r, z, t)$. The region around $r = z = 0$ is treated by softening the gravitational potential as $\phi = -1/(r^2 + z^2 + \epsilon^2)^{1/2}$.

3.3. *Adopted Initial Model*

The initial model we assume in the simulations is given by the model expressions for the density, temperature, and magnetic field, as well as the gravitational potential, as follows.

3.3.1. *Central Source of Gravity*

We assume as stated above that a massive central object with $M \sim 10^9\ M_\odot$ and a geometrically thick gas disk of much smaller mass is rotating around it. We neglect the self-gravity of the disk and assume that the gravity is due solely to the central object. As we deal with the phase in which the accreted mass flows toward the center and

forms a disk due to the loss of angular momentum, we assume that the inner radius of the disk is still far from the Schwarzschild radius, and therefore the effect of general relativity is not important in our case.

3.3.2. *Geometrically Thick Disk Model and Its Rotation Law*

The full simulation of collapse evolution is not yet undertaken. We therefore choose to study a physically plausible intermediate stage of the evolution of the system where a dense cloud of gas and associated field forms around the central massive object. We begin our calculation by approximating this stage of the evolution by a doughnut-like thick disk (see, e.g., Abramowicz et al. 1978). Exact solutions can be obtained under the simplifying assumptions for the distributions of angular momentum and pressure:

$$L = L_0 r^a , \tag{7}$$

$$P = K\rho^{1+1/n} . \tag{8}$$

Then the distribution of material in the disk will be described according to

$$\psi = -\frac{GM}{(r^2+z^2)^{1/2}} + \frac{1}{2(1-a)} L_0^2 r^{2a-2} + (n+1)\frac{P}{\rho} = \text{constant} . \tag{9}$$

The mass distribution outside the disk is assumed to be that of the high-temperature halo surrounding the black hole plus accretion disk system, created in the lowered density "cavity" from which the mass has fallen to the central object. The density must be considerably low compared to the density of disk. For the halo, we assume a constant temperature T_h, and the density distribution is assumed to obey hydrostatic law, for simplicity:

$$\rho = \rho_h \exp\left[\alpha\left(\frac{r_0}{\sqrt{r^2+z^2}} - 1\right)\right], \tag{10}$$

where $\alpha = (GM/RT_h)/r_0$ and ρ_h is density at an appropriate radius r_0. The halo is assumed to be nonrotating at $t = 0$. The boundary between the disk and halo is initially so "tailored" that the pressure equilibrium holds between the disk and the halo. By simulating the evolution of a nonmagnetized disk starting from the initial condition stated above, we confirmed that the small deviation from equilibrium of such an initial state only leads to a small disturbance in the halo with maximum speed $0.3v_{\varphi 0}$. The disturbance inside the disk is much smaller. The density distribution of the disk does not change significantly over three rotation periods. Such stability of the nonmagnetized geometrically thick disk is partly due to the assumption of axisymmetry. It is known that geometrically thick disks are dynamically unstable against nonaxisymmetric perturbations (Papaloizou & Pringle 1984). The existence of a geometrically thick disk may be transient but cannot be ruled out because three-dimensional hydrodynamical simulations (Hawley 1991) showed that when the general relativistic effects are taken into account, the inflow from the inner edge of the disk reduces the growth rate and saturation level of the nonaxisymmetric instability. Since the jet formation and the avalanche flow are found to occur in our model in a timescale shorter than the growth time of the nonaxisymmetric instability, it is not unphysical to adopt the geometrically thick disk model.

3.3.3. *Magnetic Field Distribution*

The primordial magnetic field connected to the central part of the forming protogalaxies and the central poloidal part of the dynamo-generated magnetic fields can be regarded as a large-scale poloidal magnetic field with respect to our black hole plus accretion disk system. As the gas frozen to the field is accreted to form a disk, the field is deformed into an "hourglass" shape just as in the case considered by Uchida & Shibata (1985) for the case of the star formation.

In this paper, for simplicity, the magnetic field in the initial state is assumed to be uniform and parallel to the axis of the disk. It turned out that the evolution of the magnetized disk does not depend so much on the assumed shape of the initial poloidal magnetic field, because the magnetic fields outside the disk are automatically deformed into an hourglass shape by the angular momentum loss and resulting accretion in the surface layer of the disk.

3.4. *Evaluation of Similarity Coefficients A_i*

We now evaluate the nondimensional coefficients A_i, which represent the relative importance of the forces in the equation of motion, e.g., in terms of the centrifugal force. The slowly rotating interstellar (or protogalactic) gas with $\rho = 10^{-23}$ g cm^{-3} and $B = 10^{-6}$ G around 1 kpc from the galactic center infalls by the loss of angular momentum, e.g., in the shock caused in the barred potential or by the nonaxisymmetric disturbance created during the encounter galaxy interactions. If this forms a marginally bound torus ($\psi = 0$) with the radius of its density maximum at $r_0 = 1$ pc, circulating a central black hole with $10^9\ M_\odot$, we get the maximum temperature of the torus as $T_0 = (GM/r_0)(1-2a)/[(2-2a)(n+1)R]$. For a constant angular momentum torus ($a = 0$) with $n = 3$, the temperature is $T_0 = 7 \times 10^7$ K. By conservation of mass and the magnetic flux, we get $\rho_0 = 10^{-14}$ g cm^{-3} and $B_0 = 1$ G at $r_0 = 1$ pc. Then we have $v_{s0} = 1.0 \times 10^8$ cm s^{-1}, $v_{K0} = 2 \times 10^8$ cm s^{-1}, and $v_{A0} = 3 \times 10^6$ cm s^{-1} when $\gamma = 5/3$. Thus, $A_1 = 0.15$ and $A_2 = 2 \times 10^{-4}$ for $A_3 \sim 1$ ($v_{\varphi 0} \sim v_{K0}$) in the torus.

It can be said that exactly similar phenomena may occur if the coefficients are the same and the initial conditions are the same in the scaled coordinate. Although exact similarity cannot be expected in the two systems we are considering, the forming star and forming black hole, but qualitatively similar phenomena can be expected if the nondimensionalized coefficients A_i are in the conceptually similar range and the initial distributions in the scaled coordinates are similar to each other's.

4. RESULTS OF SIMULATIONS AND THEIR ASTROPHYSICAL SIGNIFICANCE

Here we present results of simulations for a typical model and discuss their astrophysical significance. The parameters of the model are $a = 0$, $n = 3$, $\gamma = 5/3$, $A_1 = 0.05$, $A_2 = 1.2 \times 10^{-3}$, $A_3 = 1$, $\alpha = 5/3$, $\rho_h/\rho_0 = 10^{-3}$, and $\epsilon = 0.15r_0$. The characteristic length r_0 is chosen as the radius of the density maximum in thick disk given by $r_0 = (L_0^2/GM)^{1/(1-2a)}$. The initial magnetic field is uniform and parallel to the z-axis. The ratio of gas pressure to magnetic pressure in the halo at (0, 0, r_0) is $\beta_h = 8\pi\rho_h RT_h/B_h^2 = (2/\alpha)(\rho_h/\rho_0)/A_2 = 1.0$. The plasma β at disk density maximum (r_0, 0, 0) is $\beta_0 = 8\pi\rho_0 RT_0/B_0^2 = 2A_1/A_2 = 83$. The minimum grid size is $0.01r_0$, and the number of grid

points used is 141 × 141. The grid spacing is stretched with r and z. The size of the computational domain is $(R_{max}, Z_{max}) = (2.5r_0, 4.5r_0)$.

4.1. *Formation of Jets*

It is seen from the typical example in Figure 1 that a phenomenon qualitatively similar to that in the case of bipolar flows in star forming regions dealt with by Uchida & Shibata (1985) actually takes place also in the case studied here: B_φ is created due to the effect of differential rotation and escapes out from the disk surface along the poloidal field. (Initial weak disturbance corresponds to the onset of the rotation of the disk at $t = 0$. It is a real effect numerically but not important astrophysically). Figure 2 shows a close-up of the central region.

It is interesting to note that the toroidal field is created

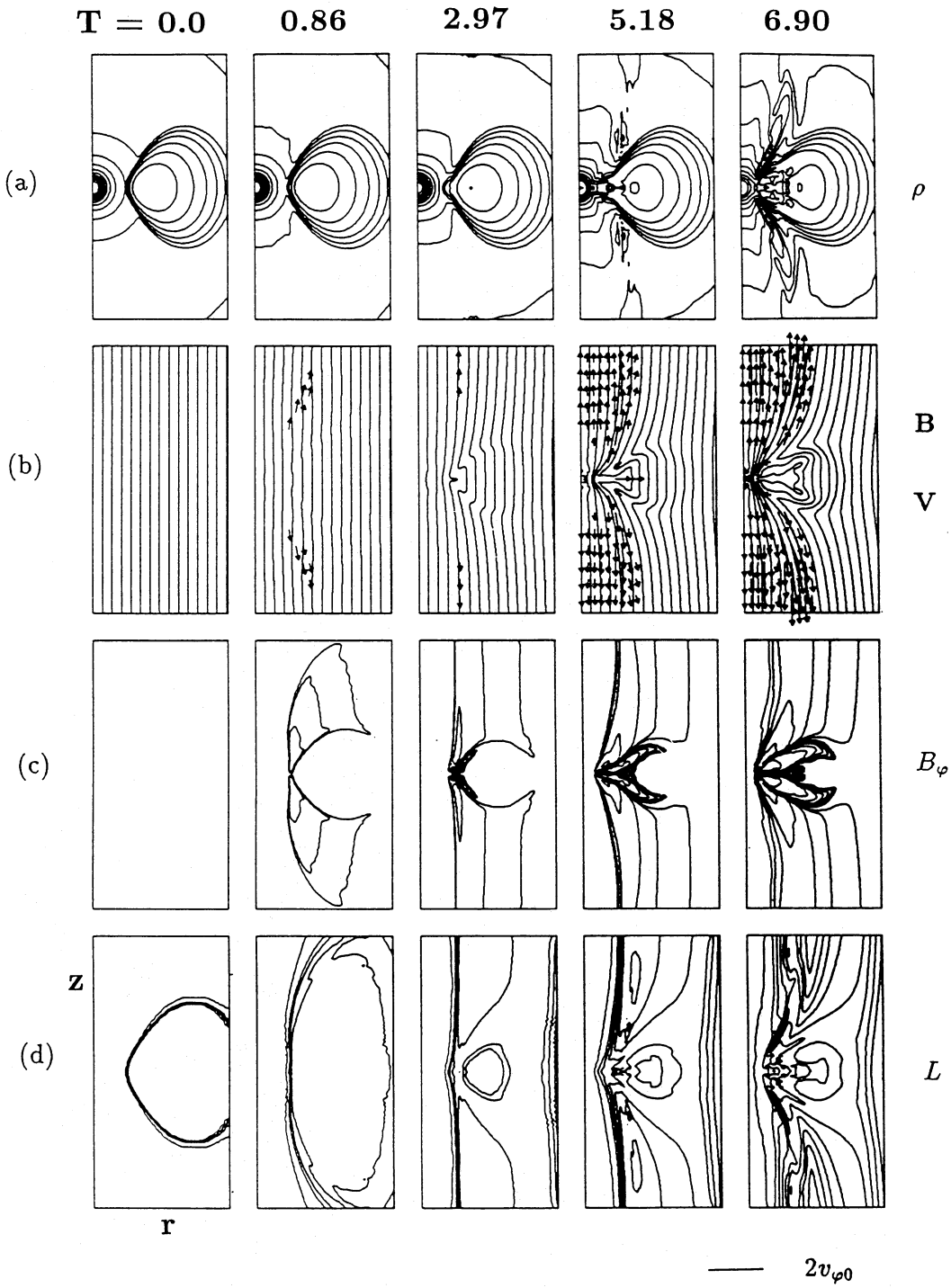

FIG. 1.—Result of numerical simulation for a typical model ($a = 0$, $n = 3$, $\gamma = 5/3$, $A_1 = 0.05$, $A_2 = 1.2 \times 10^{-3}$, $A_3 = 1$, $\alpha = 5/3$, and $\rho_h/\rho_0 = 10^{-3}$). The numbers at the top show time in units of $r_0/v_{\varphi 0}$. The plotted area corresponds to $0 < r < 2.5r_0$, and $-2.5r_0 < z < 2.5r_0$. (*a*) Density isocontours. The contour step width is 0.5 in logarithmic scale. (*b*) Poloidal magnetic field lines (*solid curves*) and the velocity vectors (*arrows*). The reference length of the velocity vectors is shown at the right bottom of the figures. (*c*) Isocontours of the strength of toroidal magnetic fields (B_φ). The contour step width is 0.25 in logarithmic scale. The toroidal field changes its direction near the surface of the disk, where the contour curves are close to each other. (*d*) Isocontours of the specific angular momentum. The step width of the contours is $0.25L_0$ in the linear scale.

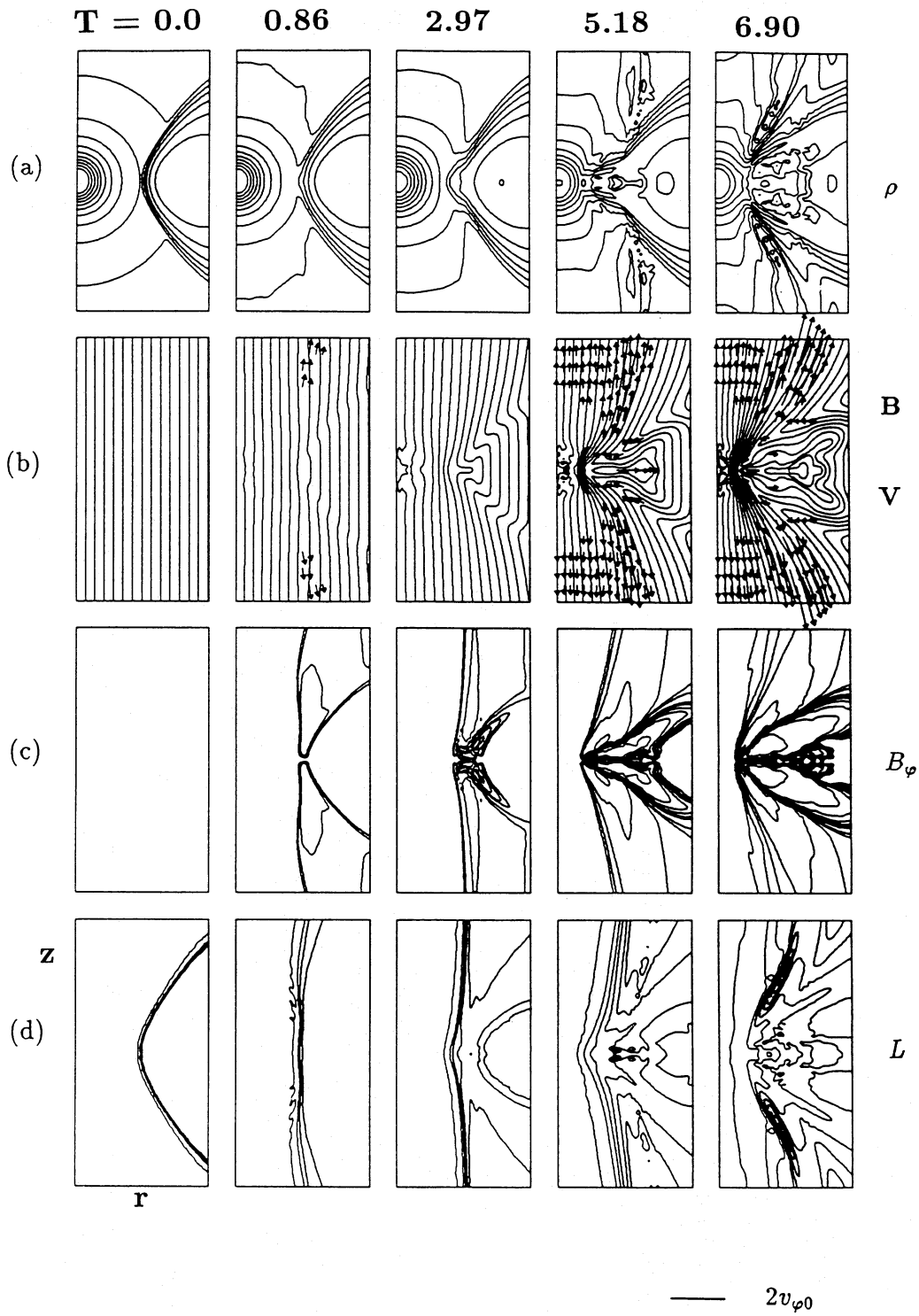

FIG. 2.—Same as Fig. 1 but for $0 < r < 1.25r_0$ and $-1.25r_0 < z < 1.25r_0$

mainly in the surface layers in which the radial magnetic field generated by the avalanche-like flow feels a differential velocity field. As the magnetic twist accumulates, it begins to relax and escape from the surface of the disk in the form of large-amplitude torsional Alfvén waves. As the waves pass through the lower density outer part of the disk (disk atmosphere), the mass in these layers as well as in the halo is entrained into the bipolar direction due to the Lorentz force in the relaxing twist. The relaxing velocity of the torsional Alfvén wave becomes larger than the free-fall velocity there, and the gas frozen-in to the field is carried upward with the relaxing twist in a helical path. The velocity is determined by the propagation velocity of the nonlinear torsional Alfvén wave. In this model, the maximum speed of the jet ($\sim 2.0v_{\varphi 0}$) is close to the rotation speed at the innermost radius of the disk, similar to the result of Shibata & Uchida (1986) for jets from geometrically thin disks. This result is also consistent with the terminal velocities obtained from a 1.5-dimensional analysis of the steady, magnetically driven jets from accretion disks (Kudoh & Shibata 1995).

4.2. *Angular Momentum Loss and Enhancement of Accretion, Leading to the Enhancement of Energy Liberation at the Center*

The loss of angular momentum of the disk material by the emission of nonlinear torsional Alfvén waves loaded by the spinning flow actually influences the disk by enhancing the rate of mass accretion to the central object. The mass infalling toward the central object is in the base part of these surface layers (driving layer) since that is the region from which angular momentum is extracted most efficiently by magnetic tension and given to the material accelerated to form jets. The denser main body of the disk has too large an inertia to be influenced readily.

It should be noted that the rotation velocity of the infalling material that has lost angular momentum increases and the rates of production of B_φ as well as of the loss of angular momentum also increase as the process proceeds. As the B_φ component increases, the infalling avalanching layer gives angular momentum to the layer below it. Thus, the dense equatorial part of the disk is pressed outward (toward large radii) at the expense of the infalling driving layers near the surface. In Figure 2 at $t = 5.18 r_0/v_{\varphi 0}$, we can see the infalling motion in the surface layer with speed $\sim 0.3 v_{\varphi 0}$ and the outward motion of the equatorial part of the disk.

The magnetic field lines at $t = 6.90 r_0/v_{\varphi 0}$ show wiggling structure in the most dense part of the disk. Such deformation of initially straight magnetic field lines in high-β region ($\beta \sim 80$) occurs by the Balbus & Hawley instability (Velikhov 1959; Chandrasekhar 1961; Balbus & Hawley 1991). We shall discuss the relation between the Uchida-Shibata model and the Balbus & Hawley instability later, in § 5.

We now try to see how the loss of angular momentum due to the production of finite-amplitude torsional Alfvén waves accompanying spinning flow with it causes the liberation of gravitational energy at the central part. Since the process of angular momentum transfer takes place via magnetic stress, we try to see it by considering a magnetic flux tube. We take the Lagrangian coordinates for the fluid elements along the flux tube, and follow the dynamical behavior of these fluid elements to evaluate the exchange of angular momentum.

Figure 3*a* shows the changes in time of the Eulerian coordinates of Lagrangian fluid elements in the meridional plane. Figure 3*b* shows the time variation of Lagrangian

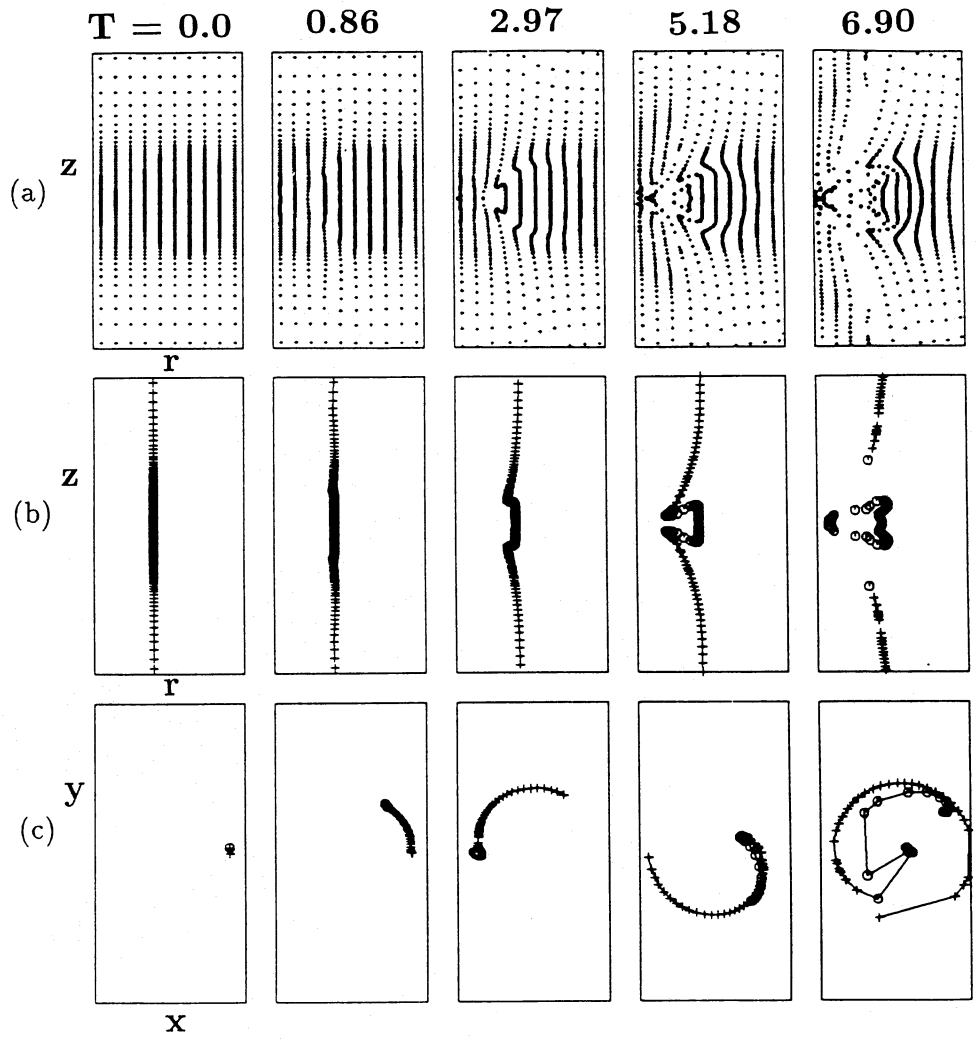

FIG. 3.—Time variation of the position of Lagrangian fluid elements. The circles denote the fluid elements that are initially located in the denser part of the disk where $\rho/\rho_0 > 10^{-2}$. Numbers at the top show time in unit of $r_0/v_{\varphi 0}$. (*a*) Projection on the meridional plane. The plotted area is $0 < r < 2.5 r_0$ and $-2.50 r_0 < z < 2.50 r_0$. (*b*) Lagrangian fluid elements along a magnetic flux tube that are initially located at $r = r_0$. (*c*) Projection of the location of the same Lagrangian fluid elements on the equatorial plane. The plotted area is $-1.25 r_0 < x < 1.25 r_0$ and $-2.50 r_0 < y < 2.50 r_0$.

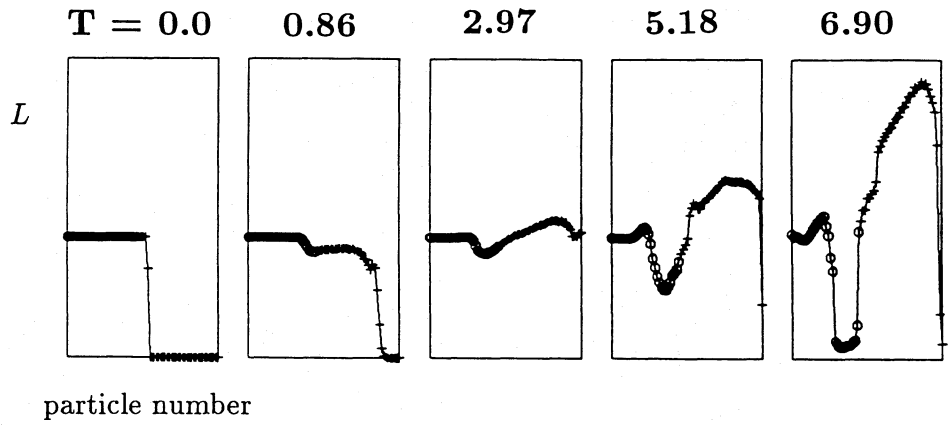

FIG. 4.—Variation of the specific angular momentum carried by the Lagrangian fluid elements shown in Fig. 3*b*. The x coordinate is the Lagrangian coordinate of the fluid elements. Numbers at the top show time in unit of $r_0/v_{\varphi 0}$. Circles denote the fluid elements that are initially located in the denser part of the disk ($\rho/\rho_0 > 10^{-2}$). The discontinuity at $t = 0$ corresponds to the interface between the rotating disk and the nonrotating halo.

fluid elements along a magnetic flux tube. In these figures, circles denote the fluid elements initially located in the denser part of the disk where $\rho/\rho_0 > 10^{-2}$. They show that the elements in the surface layers slide down along the surface toward the central object, whereas those fluid elements ranging from the low-density outer layers of the disk to the halo part are driven outward as time progresses. About 5% of the mass in the flux tube shown in Figure 3*b* has accreted to the central object in one rotation time of the most dense part of the disk.

Figure 3*c* shows the projection on the equatorial plane in which the flux tube is wound up due to the differential rotation of the disk, the fluid elements in the disk pull the flux tube together with the fluid elements on the outer parts into rotation, and the elements in the outer part move away from the axis.

Figure 4 shows the variation of the specific angular momentum carried by the fluid elements with the Lagrangian coordinate in the x coordinate. The early stage at $t = 0.86r_0/v_{\varphi 0}$ is similar to the early stage of the evolution of field aligned rotator, which Mouschovias & Paleologou (1980) studied without including the effect of differential rotation of the disk. In the later stage, the angular momentum of the disk is given to the material outside the surface of the disk via magnetic stress. The rotation of the outside elements are accelerated through magnetic stress, while the elements in the surface layer are braked by the magnetic stress compared with the initial equilibrium value (magnetic braking). It is clear that the magnetically braked fluid element can continue to fall, liberating gravitational energy further and ejecting the jets stronger.

4.3. *Dependence on the Initial Magnetic Field Strength*

In this subsection we show the dependence of numerical results on the initial magnetic field strength. Table 1 shows the models and some numerical results. The disk parameters are $a = 0$, $n = 3$, $\gamma = 5/3$, $A_1 = 0.05$, and $A_3 = 1$ for all models. The parameters for the spherical halo are $\alpha = 1.0$ and $\rho_h/\rho_0 = 10^{-2}$ (model B1) or $\rho_h/\rho_0 = 10^{-3}$ (models B2–B5). The softening parameter of the gravitational potential is $\epsilon = 0.20r_0$. The number of grid points is 201 × 201. The grid size is $\Delta r = 0.01$ when $0 < r < 1.0$ and $\Delta z = 0.01$ when $0 < z < 1.0$. Figure 5 shows the isocontours of density, toroidal magnetic field, poloidal velocity vectors, and poloidal magnetic field lines after one rotation ($t \sim 2\pi r_0/v_{\varphi 0}$). We find that the jet speed ($V_{\rm jet}$) is determined primarily by the rotation speed at the inner edge of the disk and that it only weakly depends on the initial magnetic field strength. The avalanche motion is more prominent in high-β disks (models B2–B5). In the low-β disk (model B1) the accretion speed is fastest in the equatorial plane. The growth time of the avalanche is shorter than one rotation period and almost independent of β. This property is similar to that of the Balbus & Hawley instability, where the growth rate is independent of the strength of the poloidal magnetic fields (Balbus & Hawley 1991).

The seventh and the eighth column of Table 1 show the base height of the avalanching layer at $r = r_0$ and the ratio

TABLE 1

THE MODEL PARAMETERS AND SOME NUMERICAL RESULTS

Model	A_2	ρ_h/ρ_0	β_h	β_0	$V_{\rm jet}/V_{\varphi 0}$	$Z_{\rm av}/r_0$	$M_{\rm av}/M_{\rm tot}$	$\beta_{\rm av}$	$M_{\rm jet}/M_{\rm tot}$
B1.....	0.10	10^{-2}	0.2	1.0	1.2	0.0	0.84	1.0	0.10
B2.....	6.7×10^{-3}	10^{-3}	0.3	15	2.3	0.21	0.26	10	0.020
B3.....	1.0×10^{-3}	10^{-3}	2.0	100	1.7	0.45	0.050	10	0.007
B4.....	2.0×10^{-4}	10^{-3}	10	500	1.1	0.52	0.013	20	0.0034
B5.....	2.0×10^{-5}	10^{-3}	100	5000	0.6	0.60	0.0015	100	0.0008

NOTE.—The numerical results are at $t = 6.3r_0/v_{\varphi 0}$ (one rotation). The second column shows $A_2 = v_{A0}^2/v_{\varphi 0}^2$. The fourth column denotes the halo plasma β defined as $\beta_h = 8\pi\rho_h RT_h/B_h^2 = (2/\alpha)(\rho_h/\rho_0)/A_2$, where $\alpha = 1$ for all models. The fifth column is the disk plasma β defined as $\beta_0 = 8\pi\rho_0 RT_0/B_0^2 = 2A_1/A_2$, where $A_1 = v_{s0}^2/(\gamma v_{\varphi 0}^2) = 0.05$ for all models. $V_{\rm jet}$ is the maximum speed of the jet, $Z_{\rm av}$, $M_{\rm av}$, and $\beta_{\rm av}$ are the base height of the avalanche, the ratio of the mass involved in the avalanche to the total mass $M_{\rm tot}$ inside the flux tube initially located at $r = r_0$, and the initial plasma β at the base of the avalanche, respectively. The last column shows the mass fraction of the accelerated jet.

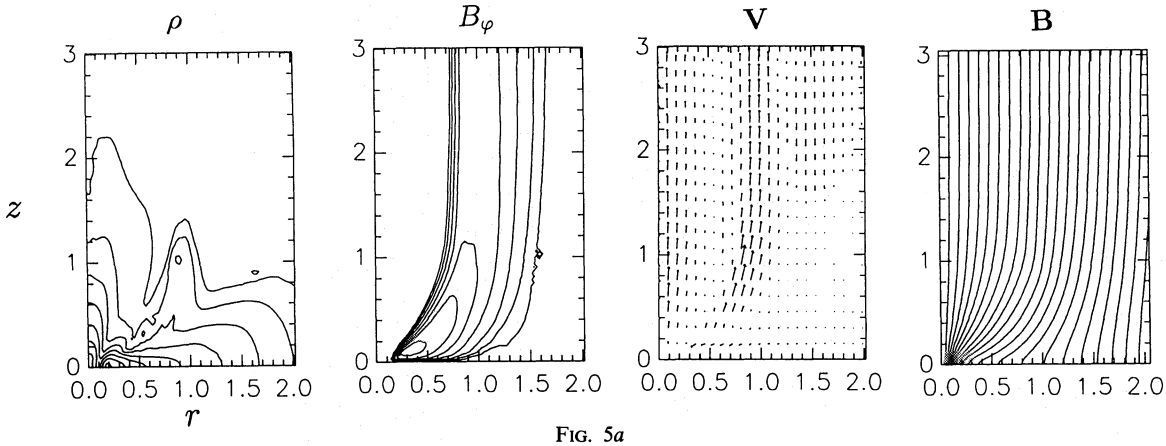

FIG. 5*a*

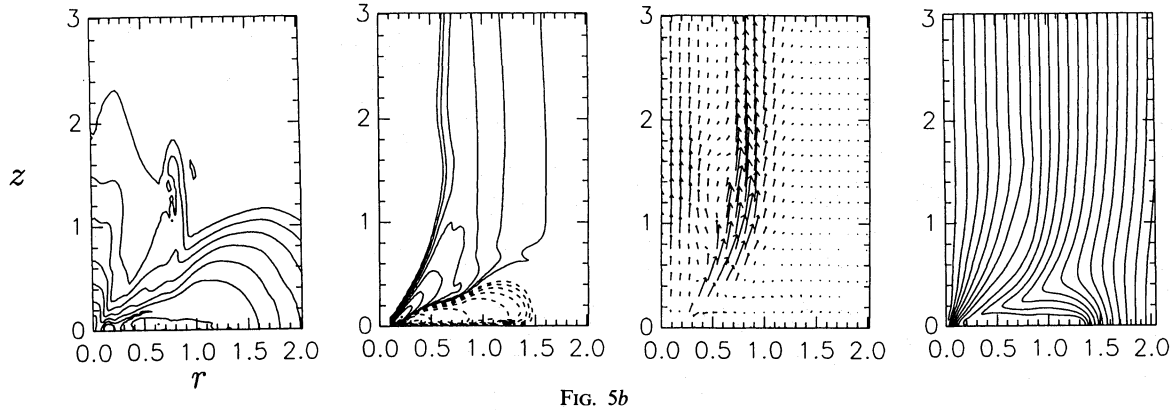

FIG. 5*b*

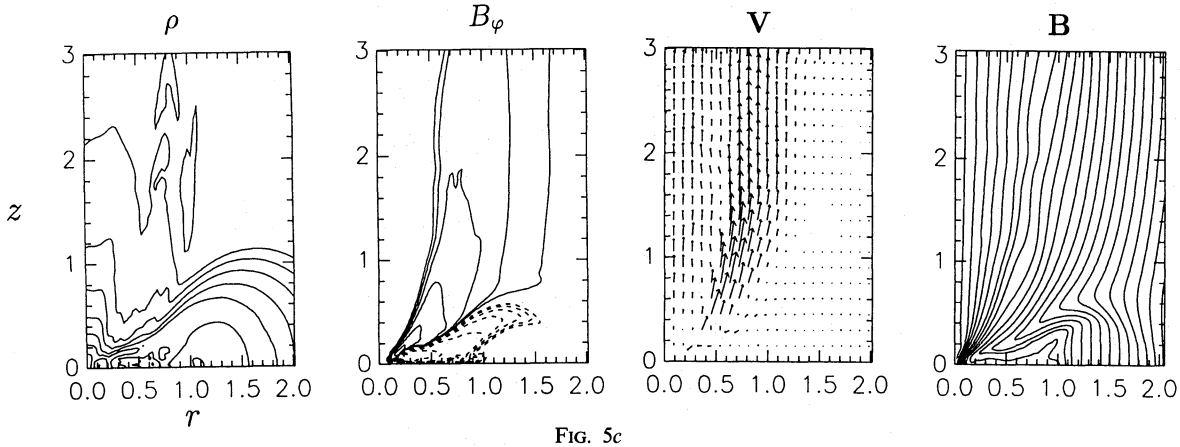

FIG. 5*c*

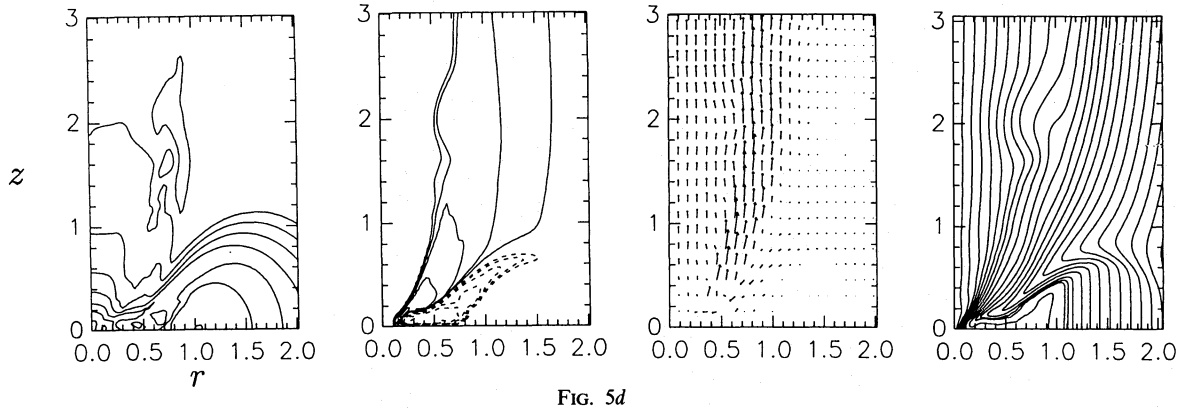

FIG. 5*d*

FIG. 5.—The density isocontours, isocontours of toroidal magnetic fields, poloidal velocity vectors, and the poloidal magnetic field lines after one rotation for (*a*) model B1 ($A_2 = 0.10$), (*b*) model B2 ($A_2 = 6.7 \times 10^{-3}$), (*c*) model B3 ($A_2 = 1.0 \times 10^{-3}$), (*d*) model B4 ($A_2 = 2.0 \times 10^{-4}$), and (*e*) model B5 ($A_2 = 2.0 \times 10^{-5}$). Other disk parameters are $a = 0$, $n = 3$, $\gamma = 5/3$, $A_1 = 0.05$, and $A_3 = 1$ for all models. The contour step width for density is 0.5 in logarithmic scale. The dashed curves and solid curves in the isocontours of toroidal field correspond to the different polarity. The contour step width for the toroidal magnetic field is 0.25 in logarithmic scale. The reference length of velocity vectors is shown at the bottom of the figures.

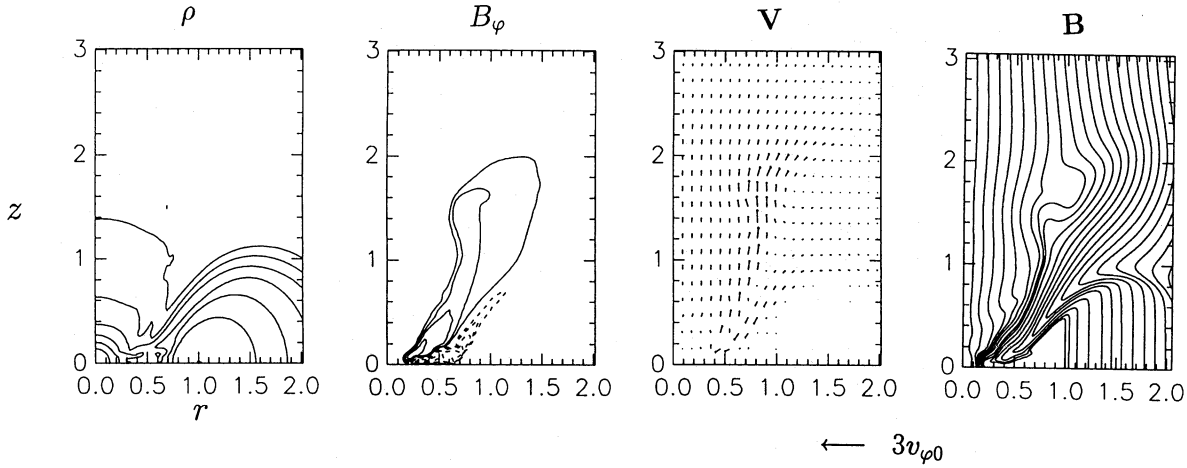

FIG. 5e

of the mass involved in the avalanche (M_{av}) to the total mass (M_{tot}) inside the flux tube initially located at $r = r_0$. The avalanching mass is approximately given by $M_{av}/M_{tot} \sim 0.1/\beta_h$. When the initial magnetic field is strong ($\beta_0 \sim 1$), almost all the mass accretes to the central object in a dynamical timescale by magnetic braking. This result is consistent with the numerical results by Shibata & Uchida (1986) and Stone & Norman (1994) starting from the geometrically thin, Keplerian disks. When $\beta_h > 10$, the avalanche occurs in a thin layer close to the interface between the disk and the halo. On the other hand, when $\beta_h < 10$, the avalanche layer locates deep inside the accretion disk where $\beta \sim 10$. Since the avalanche occurs by the extraction of the angular momentum by magnetic torque, it happens when the tension force $B_z^2/(4\pi\rho r_c)$, where r_c is the curvature radius of magnetic field lines, is comparable to the centrifugal force $v_{\varphi 0}^2/r_0$. By equating these forces, we obtain $\beta_{av} \sim (\gamma/2)(r_c/r_0)(v_{s0}/v_s)^2/A_1 \sim 10$. This expression for β_{av} is consistent with numerical results. The accretion rate by avalanche flow is proportional to the total mass of the disk above the base height of the avalanche layer where $\beta \sim \beta_{av}$. The last column of Table 1 shows the ratio of the mass ejected as jets to the total mass of the flux tube initially located at $r = r_0$. When $\beta_h < 10$, about 10% of the accreting mass is ejected as jets.

5. DISCUSSION

We have shown that jets are actually formed in the massive central object and the accretion disk at the center of protogalaxies (or galaxies with significant mass and magnetic field accretion) by the same mechanism that we called the sweeping magnetic twist mechanism. The calculation naturally includes the centrifugal acceleration of the fluid elements in a self-consistently deforming flux tube and deals with the real nonlinear magnetohydrodynamics of the system. We include such effects as the nonlinear pinching effects that modify the shape of the system drastically as the disturbance progresses, or the back-reaction of the angular momentum loss to the disk rotation, etc., which we have noted in the case of the star formation.

This is what we claimed from the similarity in the nondimensionalized MHD equations (Uchida & Shibata 1986), because the nondimensionalized set of equations become nearly identical (in a very rough sense) for these jet phenomena. The relative importance of the terms (represented by the set of A_i's) is conceptually similar in the sense that the magnetic field is passively wound up but is still extracting angular momentum from the disk. The initial distributions of quantities (e.g., initial configuration of the central object and disk) are similar, at the corresponding points in the scaled coordinates for the respective cases.

For the fiducial parameters given here, the calculation is nonrelativistic and we are able to identify a number of interesting physical points. If we want to study these processes closer to the central black hole, then a fully relativistic calculation (see, e.g., Evans & Hawley 1988) would be demanded. We are strongly motivated to pursue this in future work since it is observed that VLBI jets are relativistic with bulk Lorentz factors of order a few on subparsec scales. We suspect that the magnetic processes will still dominate in the relativistic regime. The full general relativistic calculation with Kerr Black hole is probably necessary to produce the above-mentioned Lorentz factors.

Numerical simulations using a 2.5-dimensional MHD code showed that when the differentially rotating disk is threaded by large-scale weak poloidal magnetic field ($\beta_0 > 10$), the surface layer of the disk accretes faster than the equatorial part due to the angular momentum loss through the emission of torsional Alfvén waves. The surface accretion flow generates radial magnetic fields from the poloidal magnetic field, while the radial magnetic field creates toroidal magnetic fields by differential rotation. When the magnetic twists are accumulated in the surface layer of the disk, they relax along the large-scale magnetic field as torsional Alfvén waves, extracting the angular momentum from the surface layer and enhancing the radial accretion. This positive feedback mechanism creates avalanche-like flow in surface layer of accretion disks. The magnetic field lines are automatically deformed into an hourglass shape assumed as an initial condition in our previous study (Uchida et al. 1991). The matter in the infalling surface layer accretes to the central object in the timescale of one rotation of the disk. The amount of the disk gas involved in this avalanche is 5%–10% of the total mass inside the radius of the torus (r_0) when the plasma β around the disk-halo interface is near unity. The avalanche mass decreases when β increases. The amount of the matter accelerated as jets is about 10% of the accreting mass when $\beta_h \sim 1$. The energy source of the acceleration of the jet is the gravitational energy released by the infalling matter in the avalanche flow.

Thus, we infer that when the accretion disk in AGNs is $10^7\ M_\odot$ inside a radius of 1 pc from a central $10^9\ M_\odot$ black

hole, the accretion rate by avalanche flow at 5% efficiency at 30% of the free-fall velocity is roughly 300 $M_\odot$ yr^{-1}, which is sufficient to explain the luminosity of AGNs of order 10^{47}–10^{48} ergs s^{-1} if the liberated gravitational energy is converted to radiation near the black hole with a 1%–10% efficiency.

Here we shall comment on the relation between the mechanism of the avalanche flow and the Balbus & Hawley instability (see, e.g., Balbus & Hawley 1991, 1992; Hawley & Balbus 1991, 1992), which has been studied extensively as a promising mechanism of the angular momentum transport *inside* accretion disks. Our mechanism, which was actually discussed (Uchida & Shibata 1985; Shibata & Uchida 1986) earlier than the above local treatment, is a global *nonlinear* version of the same physical process. In our model, the effect of the vertical stratification of the disk is included. Also, the torsional Alfvén waves that cause the Balbus & Hawley instability propagating out in bipolar directions are important in our model. They create jets by entraining the matter in the low-density part of the disk into a spinning flow and also cause the through continued extraction of angular momentum from the disk surface (magnetic braking). The avalanche flow that appeared in our simulation corresponds to the two-channel flow found in the nonlinear local simulations of the axisymmetric Balbus & Hawley instability (Hawley & Balbus 1992). In the local incompressible limit, Goodman & Xu (1994) found an exact solution of axisymmetric Balbus & Hawley instability, which grows exponentially in the nonlinear stage. The resulting predominantly toroidal field can also be subjected to the nonaxisymmetric Balbus & Hawley instability (Balbus & Hawley 1992; Vishniac & Diamond 1992; Hawley et al. 1995; Matsumoto & Tajima 1995; Brandenburg et al. 1995) and other parasitic instabilities (Goodman & Xu 1994). Since we assumed axial symmetry, such nonaxisymmetric effects are not taken into account in the simulations presented in this paper. Three-dimensional MHD simulations of the Balbus & Hawley instability under a local shearing box approximation (Hawley et al. 1995; Matsumoto & Tajima 1995) really showed that in high-β disks, the two channel flow breaks up by nonaxisymmetric effects. A work is now in progress to answer the question whether in three dimensions the avalanche flow continues or breaks up after several rotations. If the avalanche flow breaks up by nonaxisymmetric instabilities, it can generate turbulence in the surface layer of accretion disks. We will report the results of such three-dimensional global MHD simulations in subsequent papers.

We showed in this paper that angular momentum is exchanged between the infalling matter in the surface layer and the outgoing matter in the jet through the action of the magnetic fields. The angular momentum extraction by the emission of torsional Alfvén waves (magnetic braking) was discussed by Mouschovias & Paleologou (1980) using a one-dimensional approximation of field aligned rotator. The avalanche flow was not found in their analysis because they did not consider the differential rotation of the disk in radial direction. More quantitative analysis of magnetic braking in differentially rotating disks using the shearing sheet model will be reported in a separate paper.

An interesting problem is the detailed behavior of the gas and magnetic field at the inner edge of the disk. The avalanching material pulling the deformed magnetic field with it may cause an interesting magnetic interaction at the tip of the inner edge of the disk where the avalanches coming from the upper and lower surfaces meet. The polarities of the magnetic field brought in these avalanches to the meeting point are opposite, and magnetic reconnection may take place. This magnetic reconnection may give a new mechanism for the acceleration of nonthermal particles provided for the jets and lobes.

A question about this calculation that is often discussed is what is the steady state after all the initial conditions and transients have had time to settle down. Our view is that a steady state can be reached if there is a continuous supply of matter and field to the disk. Conceptually, there will be a steady output of power along the jet caused by the Poynting flux of the torsional Alfvén waves. We are unable to carry our calculation to the point where the steady state is achieved due to the development of as yet unavoidable numerical instabilities in a very long time computation. We suspect the principal uncertainty is the field topology, since at the end of our calculations we can see that reconnection may occur and a topology change in the field structure may result. This could have interesting implications for the final steady state structure of the outflow. We hope to be able to study this further.

The authors thank R. Rosner, H. Spruit, T. Tajima, A. Valinia, Y. Todo, and H. Ando for helpful discussions. Numerical computations were performed using Facom VP200 and VPX at the National Institute of Fusion Science, HITAC S820/80 at the Computer Center of the University of Tokyo, and Facom VPP500 at the Institute of Space and Astronautical Science. This work is in part supported by the Ministry of Education, Science, and Culture grant for the International Scientific Research Program (Joint Research No. 03044031, PI Y. Uchida) and the Scientific Research Grant of the Ministry of Education, Science, and Culture, Japan (07640348).

REFERENCES

Abramowicz, M., Jaroszynski, M., & Sikora, M. 1978, A&A, 63, 221
Balbus, S. A., & Hawley, J. F. 1991, ApJ, 376, 214
———. 1992, ApJ, 400, 610
Begelman, M. C., Blandford, R. D., & Rees, M. 1984, Rev. Mod. Phys., A56, 255
Blaes, O. M. 1987, MNRAS, 227, 975
Blandford, R. D., & Payne 1982, MNRAS, 199, 883
Brandenburg, A., Nordlund, A., Stein, R. F., & Torkelsson, U. 1995, ApJ, 446, 741
Camenzind, M. 1987, A&A, 184, 341
Cao, X., & Spruit, H. C. 1994, A&A, 287, 80
Chandrasekhar, S. 1961, in Hydrodynamic and Hydromagnetic Stability (New York: Oxford Univ. Press), 384
Contopoulos, J., & Lovelace, R. V. E. 1994, ApJ, 429, 139
Evans, C. R., & Hawley, J. F. 1988, ApJ, 332, 659
Fukue, J. 1982, PASJ, 34, 163
Goodman, J., & Xu, G. 1994, ApJ, 432, 213
Hawley, J. F. 1991, ApJ, 381, 496
Hawley, J. F., & Balbus, S. A. 1991, ApJ, 376, 223
———. 1992, ApJ, 400, 595
Hawley, J. F., Gammie, C. F., & Balbus, S. A. 1995, ApJ, 440, 742
Heyvaerts, J., & Norman, C. A. 1989, ApJ, 347, 1055
Kudoh, T., & Shibata, K. 1995, ApJ, 452, L41
———. 1996, in preparation
Kulsrud, R. M., & Andersen, S. W. 1992, ApJ, 396, 606
Li, Z. Y. 1995, ApJ, 444, 848
Lovelace, R. V. E., Mehanian, C., Mobarry, C. M., & Sulkanen, M. E. 1986, ApJS, 62, 1
Lovelace, R. V. E., Romanova, M. M., & Newman, W. I. 1994, ApJ, 437, 136

Lovelace, R. V. E., Wang, J. C. L., & Sulkanen, M. E. 1987, ApJ, 315, 504
Lubow, S. H., Papaloizou, J. C. B., & Pringle, J. E. 1994a , MNRAS, 267, 235
———. 1994b , MNRAS, 268, 1010
Lynden-Bell, D. 1978, Phys. Scr., 17, 185
Matsumoto, R., Matsuzaki, T., Hayashi, M. R., & Shibata, K. 1996, in preparation
Matsumoto, R., & Tajima, T. 1995, ApJ, 445, 767
Mestel, L. 1972, in Stellar Evolution, ed. H. Y. Chiu & A. Muriel (Cambridge: MIT Press), 643
Mouschovias, T. C., & Paleologou, E. V. 1980, ApJ, 237, 877
Papaloizou , J. C. B., & Pringle, J. E. 1984, MNRAS, 208, 721
Pudritz, R. E., & Norman, C. A. 1983, ApJ, 274, 677
Sakurai, T. 1987, PASJ, 39, 821
Shibata, K., & Uchida, Y. 1986, PASJ, 38, 631
———. 1990, PASJ, 42, 39
Stone, J. M., & Norman, M. L. 1992a, ApJS, 80, 753
Stone, J. M., & Norman, M. L. 1992b, ApJS, 80, 791
———. 1994, ApJ, 433, 746
Tagger, M., Pellat, R., & Coroniti, F. V. 1992, ApJ, 393, 708
Tout, C. A., & Pringle, J. E. 1992, MNRAS, 259, 604
Uchida, Y., Kaifu, N., Shibata, K., Hayashi, S. S., Hasegawa, T., & Hamatake, H. 1987, PASJ, 39, 907
Uchida, Y., Matsumoto, R., Hirose, S., & Shibata, K. 1991, in Primodial Nucleosynthesis and Evolution of Early Universe, ed. K. Sato & J. Andouze (Dordrecht: Kluwer), 409
Uchida, Y., & Shibata, K. 1985, PASJ, 37, 515
———. 1986, Canadian J. Phys., 64, 507
Uchida, Y., et al. 1996, in preparation
Ustyugova, G. V., Koldoba, A. V., Romanova, M. M., Chechetkin, V. M., & Lovelace, R. V. E. 1995, ApJ, 439, L39
Velikhov, E. P. 1959, Soviet Phys.–JETP Lett., 9, 995
Vishniac, E. T., & Diamond, P. 1992, ApJ, 398, 561